Materials Science & Engineering B 231 (2018) 18–27

Contents lists available at ScienceDirect

Materials Science & Engineering B

journal homepage: www.elsevier.com/locate/mseb

Direct growth of ZnO nanostructures on the Zn electroplated mild steel to create the surface roughness and improve the corrosion protection of the electroless Ni-P coating

Zahra Sharifalhoseini[a,*], Mohammad H. Entezari[a,b,*], Mohsen Shahidi[c]

[a] Sonochemical Research Center, Department of Chemistry, Ferdowsi University of Mashhad, 91779 Mashhad, Iran
[b] Environmental Chemistry Research Center, Department of Chemistry, Ferdowsi University of Mashhad, 91779 Mashhad, Iran
[c] Samed Chemical Inds. Co., Mashhad, Iran

ARTICLE INFO

Keywords:
Direct ZnO growth
Zn electroplating
Corrosion protection

ABSTRACT

The disadvantages of some methods applied to deposit or grow ZnO structures led us to conduct experiments on the direct growth of the ZnO through the new and highly applicable procedure. For this purpose, the mild steel surface after the activation was coated with a thin layer of Zn using the electroplating method. This technique eliminated the need of the pure Zn foil as a relatively expensive substrate. The conventional and sonochemical hot water treatment of as-synthesized Zn crystals for the conversion to the ZnO phases offered economic benefits because there was no need for the special pretreatment of the surface before thermal oxidation. As a practical application, as-grown ZnO structures (as the sublayer) were covered with the electroless Ni-P layer and the improvement in corrosion protection of binary Ni-P coatings with and without sublayer of ZnO was studied by the electrochemical method.

1. Introduction

Recent advances in the synthesis, modification and practical applications of nanomaterials have led to the development of nanotechnology as a new interdisciplinary area of research in many fields of human life. Modification of various matrixes with nanoparticles (NPs) using several methods such as incorporation, adsorption, deposition, coating and impregnation has offered new solutions in various fields of science [1–6]. Types of nanoparticles have received so much attention in the medical applications (e.g. wound dressing, dental filler and adhesive, drug delivery and cosmetic ingredient) [7–10]. Nano-sized organic and inorganic particles have been also extensively used in a wide range of areas, including electrochemistry, photochemistry, heterogeneous catalysis, supercapacitors and ultracapacitores [11–14]. Besides, the significant improvement in the strength and the corrosion protection of various materials modified by incorporation of nanoparticles has made nanotechnology suitable for a wide variety of engineering applications [15,16]. In spite of the positive aspects, the risks of nanomaterials to health and environmental safety should be carefully considered. Most procedures applied in nanotechnology are involving the dispersion or the production of free nanosized materials. The entry of these particles into the environment may be accompanied by harmful effects due to their increased mobility and reactivity [17]. In this regard, more attention to the preparation of fixed nanoparticles and the procedure applied to obtain them are immediate concerns.

Since in this work, the production of ZnO structures has been targeted, various synthesis methods and applications of this metal oxide have been considered. Due to unique properties of ZnO, a rich variety of physical (vapor-phase process) and chemical (solution phase) methodologies were used to synthesize various ZnO nanostructures (ZnO NSs). Furthermore, the green nanosynthesis approach, which is based on using ecofriendly reagents or biogenic process, was developed to obtain nano-scaled pure ZnO particles [18,19]. Zinc oxide due to nontoxicity and good biocompatibility is developed in biomedical applications [20,21]. Furthermore, this ceramic oxide due to high electron communication feature and near ultraviolet emission, can be used as building blocks for electronic and optoelectronic devices (e.g. solar cells, ultraviolet light emitters, lasers and sensors) [22–24]. Along with solution-based approaches such as hydrothermal, sol-gel and electrochemical deposition developed to grow or deposit ZnO thin films, some other procedures, including pulsed laser deposition (PLD), molecular beam epitaxy (MBE), chemical vapor deposition (CVD), and magnetron sputtering have been extensively used for the ZnO synthesis [25–30]. For instance, Kim et al. suggested the direct growth of vertically aligned

* Corresponding authors at: Sonochemical Research Center, Department of Chemistry, Ferdowsi University of Mashhad, 91779 Mashhad, Iran (M.H. Entezari)
E-mail addresses: z.sharif@um.ac.ir (Z. Sharifalhoseini), entezari@um.ac.ir (M.H. Entezari).

https://doi.org/10.1016/j.mseb.2018.07.001
Received 13 August 2017; Received in revised form 23 June 2018; Accepted 2 July 2018

ZnO nanorods (ZnO NRs) on the window by sputtering a seed layer of the Ga-doped ZnO and the hydrothermal method to get an antireflective, self-cleanable and electrical conductive window layer for the thin film solar cell [31]. Nandi et al. reported the growth of the vertically well aligned and separated ZnO NRs through the reactive magnetron sputtering of zinc target on Si substrate under the argon-oxygen atmosphere (in the range of 300–750 °C). The resulting ZnO thin film/nanorods obtained by their research has potential to use is in light emitting diodes, laser diodes and detectors in the near-UV range [32]. Pulsed laser deposition growth of the 3D ZnO nanowall network as another research carried out in this field for dye- sensitized solar cells (DSSCs) and biosensor applications [33].

Providing sophisticated instruments with high temperature, high vacuum, and thus high cost could be mentioned as technical limitations of these methods. To overcome these limitations, facile methods such as thermal oxidation of metallic Zn has been reported to the direct growth of ZnO NSs [34]. It seems that successful efforts made in the recent years could be useful to produce fixed nanostructures and reduce the production of free nanoparticles. The results of one research conducted on the oxidation of Zn foil at temperatures of 100–400 °C showed that the final morphology of the oxidized Zn foil (including spherical oxide grains, porous nanosheets and ZnO nanorods) is strongly dependent on the oxidation temperature [35]. In another effort, large-scale ZnO nanowire arrays were grown directly on zinc foils using the thermal oxidation in air to investigate the wetting and water adhesion properties [34]. Despite the advantages of the thermal oxidation of metallic Zn film as a simple and cost-effective method, the high crystallization temperature of Zn to ZnO form (≈300 °C), is a limitation of this method. Therefore, it is interesting to investigate the effect of surface oxidation of metallic Zn foils using hot water treatment. Little research conducted into this subject can be addressed [36,37].

In general, the use of the pure Zn foil that is relatively expensive, the need of surface treatment for the activation and the direct growth of ZnO structures, high temperature, and the long time thermal oxidation are still unfavorable factors in the thermal oxidation method. In this regard, the zinc electroplating as a relatively low cost and very popular method has been used to create a thin film of Zn on the mild steel surface in this work. It is well known that the zinc electroplating is widely applied to protect steel from corrosion due to its sacrificial nature of the Zn [38]. Applying this coating method provides a suitable surface that works as the Zn^{2+} source. The use of the resulting surface instead of the pure Zn foil (used in researches as the substrate) could be a cost-effective procedure. After the deposition of a thin layer of Zn, electrogalvanized surfaces have been taken under the hot water treatment to convert Zn to ZnO form. Indeed, the immediate hot water treatment of the as-synthesized Zn crystals created using an electroplating technique eliminates the need of the pretreatment process and surface activation before the ZnO growth. Moreover, to find the effect of the acoustic excitation of the medium on the morphology of the ZnO structures, hot water treatment has been carried out in the presence and absence of ultrasound

The chemical and thermal stability of ZnO make it a good candidate as an anticorrosive pigment in organic coatings [39], whereas its performance of this ceramic oxide in the corrosion protection of metal (and alloy coatings) has been less studied. Thereby, in this research, as a practical application, the influence of as-grown ZnO structures as the sublayer on the improvement in the corrosion protection of the binary Ni-P coating has been investigated. For this purpose, resulting surfaces have been coated by the electroless Ni-P plating (EN plating) and the corrosion resistance of target samples has been evaluated using the electrochemical method (Tafel extrapolation).

2. Experimental

2.1. Materials

Zinc acetate dehydrate ($Zn(CH_3COO)_2$, $2H_2O$), trisodium citrate ($Na_3C_6H_5O_7$), boric acid, (H_3BO_3), sodium chloride (NaCl), nickel sulfate ($NiSO_4$ $(H_2O)_6$), sodium hypophosphite ($NaPO_2H_2$), hydrochloric acid and ammonia solution (all from Merck) were used directly without further purification. The sheet of commercial mild steel was selected as the metal substrate. The chemical composition of the substrate (in wt. %) acquired by a Quantometer, (3460ARLFISONS) as follows: Fe-99.340, Cu-0.043, Sn-0.001, Co-0.007, Al-0.059, Ni-0.031, Mo-0.001, Ti-0.001, P-0.013, S-0.033, Cr-0.028, C-0.024, Si-0.058, Mn-0.387.

2.2. Metal surface pretreatment

To prepare test specimens, the steel sheet was cut to the desired dimensions (40 mm × 20 mm × 1 mm) and degreased using a mild detergent solution. Then the surface of plates was grounded with an emery paper (1200 grit, SiC). The plates after rinsing with distilled water and drying were immersed in hydrochloric acid (HCl, 12 M) for 30 s to remove the oxide layer from the metal surface. Afterward, plates were washed with distilled water and immersed into to a basic solution (NaOH, 1 M) for the neutralization of the excess acid on the surface. Finally, the test specimens were soaked into the acid solution (HCl, 0.1 M) for 2 min for the surface activation. It should be noted that the airflow leads to the rapid oxidation of the resulting surface and therefore activated plates should be transferred to the plating bath immediately.

2.3. Zn electroplating

To deposit a layer of Zn on the surface of metal substrates, plates were placed in an acid bath. The composition and parameters of the bath used for the electroplating are given in Table 1.

In the applied acid bath, zinc acetate dehydrate and sodium citrate were used as the source of Zn^{2+} ions and the complexing agent, respectively. A complexing agent by controlling the free Zn^{2+} ions improves the quality of the deposit. To enhance the electrical conductivity, sodium chloride as a conductive salt was added to the electrolyte. Additionally, boric acid was used to keep plating operation conditions stable. This component acts as a buffering agent too. After the completion of this step, electroplated samples were treated in the hot water according to the procedure described in the following sections.

2.4. Hot water treatment (thermal oxidation)

The thermal oxidation of resulting coatings was carried out for the conversion of the zinc to ZnO structures. The growth of ZnO structures from the Zn were examined in conventional conditions (without ultrasound) and under sonochemical conditions.

Table 1
The composition and operating conditions of the used Zn electroplating bath.

Deposition parameters	Amount
Concentration of $Zn(CH_3COO)_2{\cdot}2H_2O$	30.0 (g/L)
Concentration of $Na_3C_6H_5O_7$	7.5 (g/L)
Concentration of H_3BO_3	5.0 (g/L)
Concentration of NaCl	3.0 (g/L)
θ (temp.)	40 (°C)
Time	15 min
Current density	12.5 (mA/cm^2)
pH	≈ 3

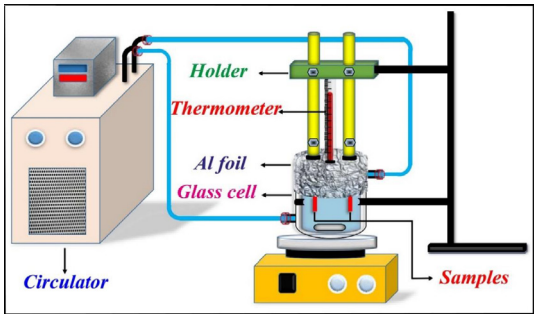

Fig. 1. Shows schematically the experimental setup used in the conventional procedure.

2.4.1. The conventional method

For this experiment, a cylindrical glass vessel containing 100 mL of distilled water was used as the reaction cell. This container was equipped with the water circulation to control the temperature, which was adjusted at 80 °C. The temperature was also checked by using an external thermometer. The samples were mounted by a Teflon holder. The top of the cell was covered with a piece of aluminum foil to reduce the heat loss. During the thermal oxidation (60 min), the medium was stirred continuously with a magnetic stirrer (300 rpm). The obtained sample was named as the sample IA. Fig. 1 is a representative schematic of the experimental setup used in this part.

2.4.2. The sonochemical method

To find the effect of the acoustic excitation of the medium on the results of the experiment, an ultrasonic apparatus equipped with an extended probe (20 kHz, model XL 2020) was used instead of the magnetic stirrer. The ultrasonic parameters, including frequency and intensity determined by the calorimetric method were 20 kHz and 35 W cm^{-2}. To reach a correct conclusion, other parameters, including time and the temperature of the reaction were the same applied in the conventional route. The sample prepared under the sonication was named as the sample IB (or sonochemical sample). The experimental setup used in this section is shown schematically in the supplementary data (Fig. 1S).

Supplementary data associated with this article can be found, in the online version, at https://doi.org/10.1016/j.mseb.2018.07.001.

2.5. Electroless Ni-P coating

To evaluate the performance of grown ZnO structures (as the sub-layer) on the corrosion protection of the Ni-P deposit, samples IA and IB were transferred to a basic Ni bath. It should be noted that low stability of the ZnO in the acid medium (its dissolution at pH < 6) limits the use of acid baths. The electroless plating was performed in the same cell described in the Section 2.4.1. The bath composition and its parameters are summarized in the Table 2.

In the applied bath, nickel sulfate was used as a source of the Ni^{2+} ions, sodium citrate as the complexing agent (to control the release of Ni^{2+} ions) and sodium hypophosphite as the reducing agent.

Table 2
The Ni-P bath composition and the parameters.

Deposition parameters	Amount
Nickel sulfate	25.0 (g/L)
Sodium citrate	7.5 (g/L)
Sodium hypophosphate	30.0 (g/L)
Lead acetate	≈ 1 ppm
θ (temp.)	70 (°C)
Time	15 min
pH	8.0–8.3

Table 3
The reaction conditions applied for the all samples.

Conditions	Step	Sample IA*	Sample IB**	Sample IIA	Sample IIB
Surface modification	1	ZnO growth	ZnO growth	ZnO growth	ZnO growth
	2	–	–	Ni-P coating	Ni-P coating
Reaction time (min)	1	60	60	60	60
	2	–	–	15	15
Temperature (°C)	1	80 ± 2	80 ± 5	80 ± 2	80 ± 2
	2	–	–	15	15

* & ** are attributed to the conventional and sonochemical methods.

Concerning the probable mechanism suggested by many researchers for the electroless Ni plating, production of H^+ ions during the coating process results in the pH reduction. Hence, the pH control during the coating is essential to prevent the bath from decomposing. For the pH adjustment, ammonia solution was used. In addition, a small amount of lead acetate was added to the bath as the stabilizer agent. After 15 min coating, samples were drawn from the bath, rinsed with distilled water and dried using a heater. Samples IA and IB after EN plating were referred to the sample IIA and IIB, respectively. The corrosion resistance of resulting samples was studied by the electrochemical method. The names and the synthesis condition of all samples are summarized in the Table 3.

2.6. Evaluation of the corrosion resistance

The electrochemical measurements were performed using a potentiostat/galvanostat (SAMA 500; Electro-analysis System) through a three-electrode setup. In the electrochemical cell configuration, a silver/silver chloride (Ag/AgCl) as the reference electrode, a platinum auxiliary electrode and the test sample as the working electrode were immersed into a beaker containing the corrosive medium (NaCl solution, 3.5 wt.%). All potentiodynamic polarization (PDP) measurements were carried after 10 min immersion to stabilize and monitor the open circuit potential (E_{OCP}). Then the potential was applied at a constant sweep rate of 1 mV/s in the range of −200 to +200 mV around the E_{OCP} and measurements were performed at room temperature. The working electrode was covered with the epoxy resin resulting in 1 cm^2 exposed area. After the collection of potentiodynamic polarization (PDP) curves, electrochemical data were extracted for all samples.

3. Results and discussion

3.1. SEM analysis of the coatings

The surface morphology of target samples was observed with a 3D microscope (LEO 1450 VP). Fig. 2(A–C) displays SEM micrographs of the steel surface after the zinc electroplating. (SEM images of the bare steel surface are shown in the supplementary data, Fig. 2S).

The images exhibit that the overall surface of the mild steel surface was covered with a zinc layer (EDS analysis confirmed the presence of the zinc element, see the Section 3.2). The intertwined Zn structures can be seen at high magnification (Fig. 2(C)). The surface morphology of this specimen after the classical hot water treatment (sample IA) is shown in Fig. 3(A–C).

From SEM images, especially at high magnification view (Fig. 3(B), the formation of the micro- and nano-sized rod-like and flower-like ZnO structures are obviously observed. The conversion of zinc to zinc oxide through the simple, cost effective, free seed and free catalyst at the relatively low temperature and the relatively short time (compared to other scientific reports) confirmed the good efficiency of the classical way to produce zinc oxide structures.

Fig. 4(A–C) presents SEM micrographs of the Zn electroplated

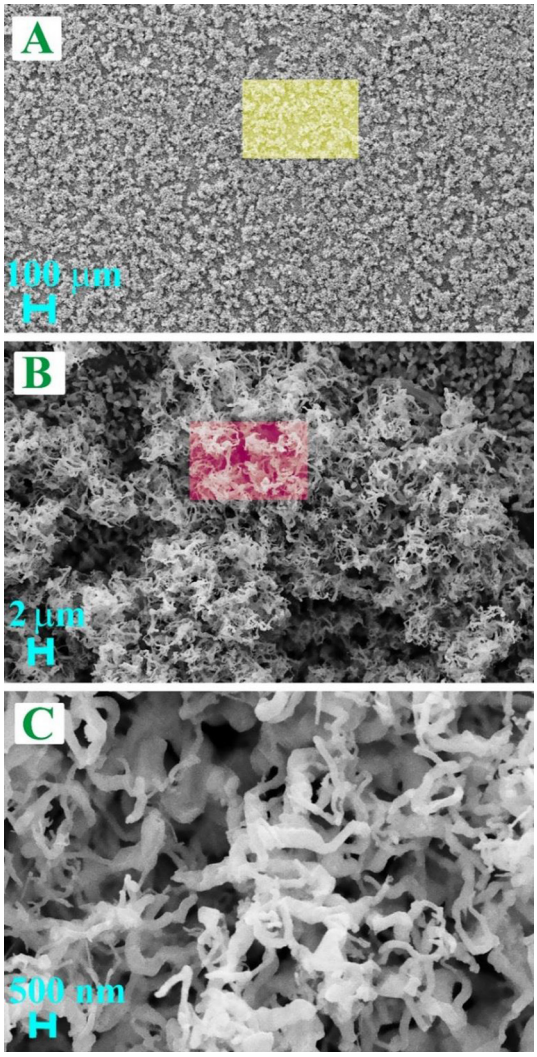

Fig. 2. The SEM images of the steel surface after Zn electroplating. (B) is related to the yellow area marked on the image (A), and (C) is a magnified view of the red area marked on the image (B), respectively.

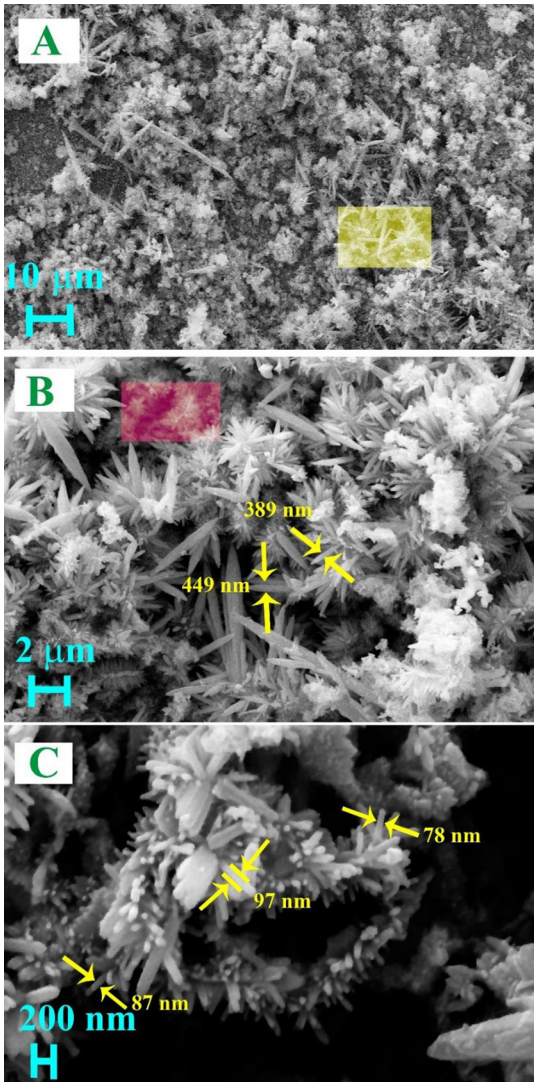

Fig. 3. The SEM micrographs of the sample IA. (B) is a magnification view of the yellow rectangle on the image (A).

surface after the sonochemical hot water treatment (sample IB).

The irregular polyhedrons observed in these images (especially in the Fig. 4(B) and (C)), could be assigned to either micro-sized ZnO structures or the reformed electrodeposited Zn coating. The second possibility can be illustrated by the recrystallization of the primary Zn form to the resulting feature due to the exposure of plates to harsh sonochemical conditions. On the other word, the conversion of the intertwined Zn structure (as a porous and sponge like morphology) to the compact shapes may be occurred under extreme conditions of the ultrasonic irradiation. However, due to the confirmation of the zinc and oxygen presence on this surface (see the Section 3.2) the formation of polyhedron zinc oxide shapes is possible too. Indeed, under the direct ultrasonic irradiation, the formation, growth, and implosive collapse of bubbles in the medium by the creation of harsh conditions in hot spots, including high temperature (~5000 K) and high pressure (~1800 atm), facility the significant change in the crystal orientation or converting the zinc to zinc oxide. At higher magnification (Fig. 4(C)), there is an interesting point about the growth of the nanowall ZnO structures on the polyhedrons surface. Recently, the growth of 3D ZnO nanowall has received a considerable interest for practical applications in DSSCs and PSCs (perovskite solar cells) [33,40].

The imaging study has been also performed for the sample IIB as a typical specimen covered with the Ni-P coating. The SEM micrographs of this sample (Fig. 5(A–C)) disclose the existence of many globular particles. The resulting surface is coarser than the EN plated steel surface without sublayer (of ZnO) obtained in our previous research [41]. In the structure of the previously prepared nickel-phosphorous coating (directly deposited on the bare steel), the nanostructures are not observed. Hence, it can be concluded that the nodular regions on the surface of the sample IIB resulted from the micro and nano-configurations of ZnO, which were grown under the Ni-P coating. To guide the eye, some of the nanosized regions formed on the surface of the sample IIB are marked with the yellow circles on Fig. 5(C). It should be noted that despite the positive influence of the smooth coating on the mechanical Ni-P layer, positive effects of the formation of Ni-P phase in nanosized dimension should be considered. It was expected that the creation of nanosized ZnO structures (due to higher contact area) result in the proper surface roughness and better adhesion of the top-layer coating.

3.2. EDS analysis

The chemical composition of the steel surface after Zn electroplating, this surface after the heat treatment via classical and sonochemical procedures (samples IA and IB), and the electroless Ni-P deposited surface (sample IIB) was obtained from EDS analysis (EDS

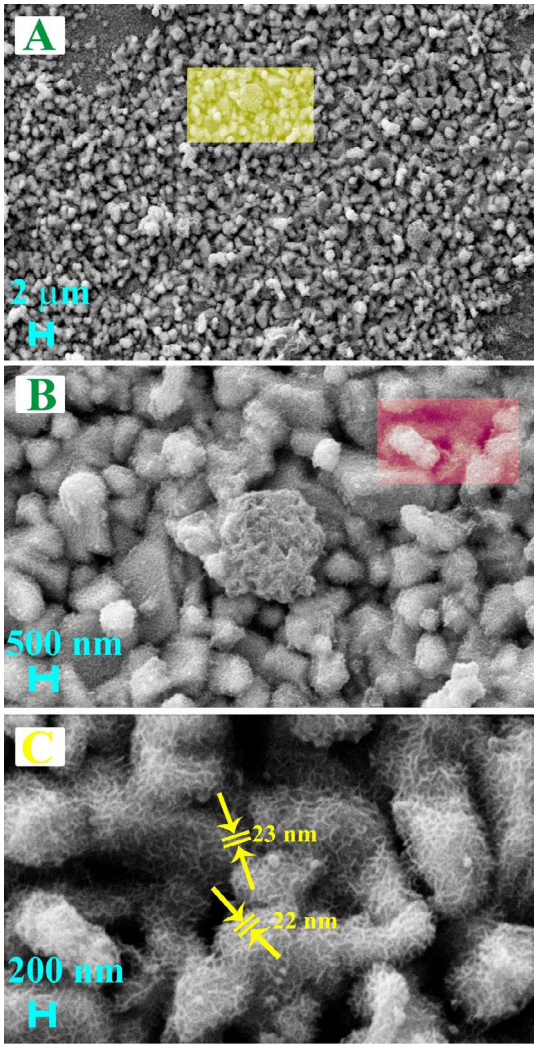

Fig. 4. The surface morphology of samples IB. (A) and (B) show the formation of the irregular polyhedron shapes in the sonochemically hot water treated sample. The growth of the nanowall ZnO structures on the polyhedrons are seen at the magnification of 50,000× (C).

equipment attached to SEM) and the results are shown in Fig. 6(A–D).

The elemental analysis using energy dispersive x-ray spectroscopy (EDS) reveals that the Zn electroplated surface contains just the zinc element (Fig. 6(A)). The results also confirm the presence of oxygen in samples IA and IB that can be regarded as an evidence for the formation of the ZnO on their surfaces (Fig. 6(B) and (C)). In the case of the sample IIB, expect elements, including nickel and phosphorus, were detected on the surface (Fig. 6(D)). For each species, the reported value of the chemical composition is attributed to the areas marked on the related SEM images. The content of the phosphorus in the Ni–P layer (sample IIB) is about 7 wt.% and measurements at other points on the surface showed the same trend, therefore this electroless deposition (according to the phosphorus content) is classified into the medium phosphorous Ni-P deposits. This category (with 4–9 wt.% phosphorous) has a smaller crystalline size and tends to be semiamorphous compared to the first category consisting of microcrystalline nickel deposits (with 1–4 wt.% phosphorous)) [42].

During the Zn electroplating two reactions mainly occur including the reduction of Zn^{2+} cations and oxidation of water as follows: At cathode:

$$Zn^{2+}(aq) + 2e^- \rightarrow Zn^0(S) \quad (1)$$

And at anode:

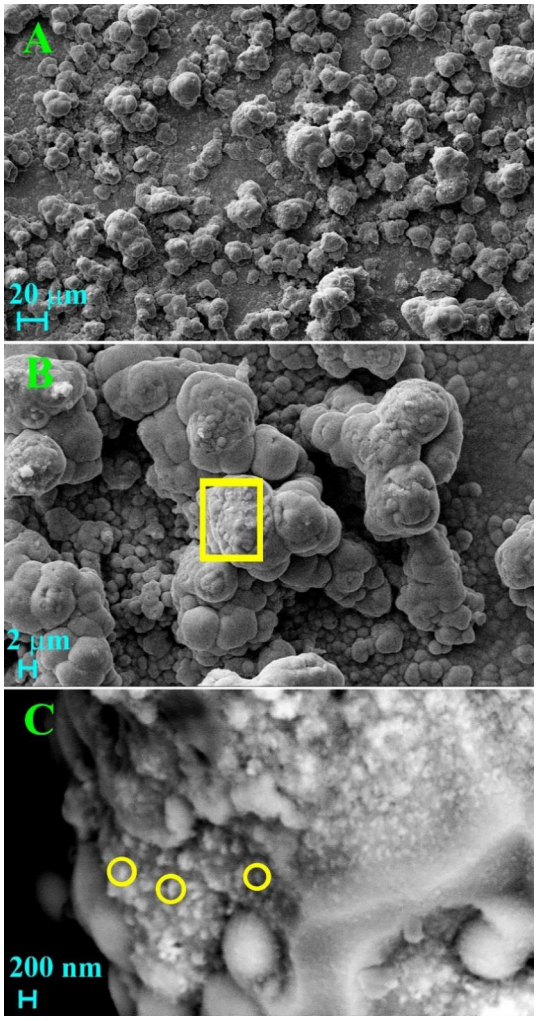

Fig. 5. The SEM images of the sample IIB. The globular particles on the surface are observed in (A) and (B). The formation of Ni-P phase in nanosized dimensions is recognized in a high magnification (C).

$$2H_2O(1) \rightarrow O_2(g) + 4H^+(aq) + 4e^- \quad (2)$$

The overall reaction could be represented as:

$$2Zn^{2+}(aq) + 2H_2O(1) \rightarrow 2Zn^0(S) + O_2(g) + 4H^+(aq) \quad (3)$$

In the case of the electroless Ni-P mechanism, the reduction of nickel in alkaline solutions follows the same pattern as in acid solutions [43]. The most probable mechanism proposed in acid bath include the adsorption of Ni^{2+} cations on active sites of the surface and chemical reduction of Ni^{2+} and P^{1+} to Ni and P in the presence of sodium hypophosphate as a reducing agent. In electroless Ni-P plating, the metallic surface acts as substrate and catalyst too. The probable mechanism can be described by the following Eqs. (4)–(7) [41,42].

$$Ni^{2+}_{ads} + H_2PO^-_{2ads} + H_2O \xrightarrow{cat} Ni^0 + 3H^+ + HPO^{2-}_3 \quad (4)$$

$$H_2PO^-_{2ads} + H_2O \xrightarrow{cat} HPO^{2-}_3 + H^+ + 2H_{ads} \quad (5)$$

$$H_2PO^-_{2ads} + H_{ads} \xrightarrow{cat} P^0 + H_2O + OH^- \quad (6)$$

$$2H_{ads} \xrightarrow{cat} H_2 \quad (7)$$

3.3. AFM analysis

The samples IA and IB were also examined by atomic force

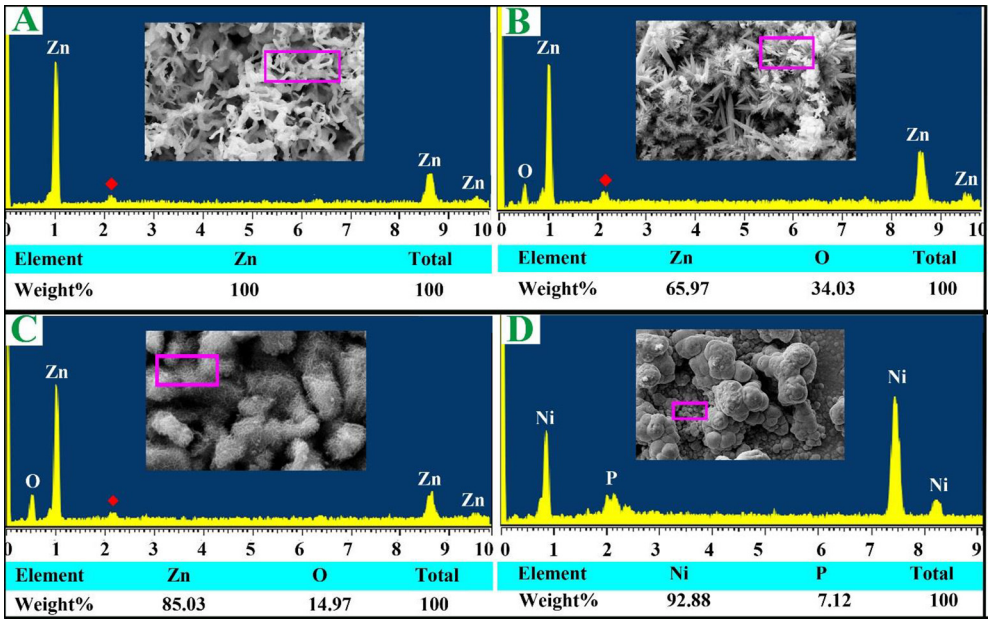

Fig. 6. The EDS spectra and chemical composition of the samples. (A) is attributed to the steel surface after Zn electroplating. (B), (C) and (D) are referred to the samples IA, IB and IIB respectively. The observation of the Au peaks (marked with red diamonds on the EDS spectra) is due to the sputter coating of the samples with gold for the SEM analysis (in the reported values, the portion of Au is omitted).

microscopy (AFM Ara research, Iran) and the results are shown in Fig. 7. This figure includes face projections (Fig. 7(A) and (D)), 3D topographies (Fig. 7(B) and (E)), and 3D phase images (C) and (F). Sample IA was labeled with (A), (B) and (C), and (D), (E) and (F) are attributed to the sample IB. The calculated roughness for the sample IA is 21 nm, and for the sample IB is 44 nm. The difference in their roughness can be attributed to the difference in the surface topography of ZnO coatings, which is obvious in their SEM images.

The Zn electroplated surface and surfaces containing ZnO NSs (samples IA and IIA) show higher roughness comparing to the bare surface. Increasing in surface roughness in mentioned samples is confirmed by SEM images. Based on scientific reports, increasing in surface roughening results in better adhesion properties of metallic film to polymer or alloy substrate [44,45].

3.4. XRD analysis

The crystal structures of samples IA and IB recorded using XRD Explorer GNR, Italia with CuKα radiation (λ = 0.154 nm) are shown in Fig. 8.

The XRD patterns of hot water treated samples (IA and IB) exhibit mixed diffraction peaks of Zn and ZnO. The peaks at 36.21, 38.91 and 43.2, corresponding to the (0 0 2), (1 0 0), and (1 0 1) planes of Zn (marked with violet, for the sample IA, ICDD no: 01-078-9363, and for the sample IB ICDD no: 04-003-5661) are attributed to the underling metallic Zn layer. Other peaks at 31.61, 34.41 and 36.21 indexed to the (1 0 0), (0 0 2), and (1 0 1) planes of ZnO (market with red color, for the sample IA, ICDD no: 04-015-4060, and for the sample IB, ICDD no: 04-013-6608) confirm the formation of ZnO phase. Note that the (0 0 2) peak of Zn overlaps with the (1 0 1) ZnO peak [36]. The presence of the (0 0 2) ZnO peak in XRD patterns shows that ZnO structures are preferentially orientated along the c-axis.

3.5. Estimation of the Zn, ZnO and Ni-P layer

By weighing samples before and after 15 min Zn electroplating, 60 min thermal oxidation and 15 min electroless plating, the amounts of Zn, ZnO and Ni-P layers were measured. To estimate the thickness of mentioned layers, all coatings were assumed uniform and the density of Zn, ZnO and binary Ni-P films considered 7.13, 5.61 and 8.00 g/cm^3, respectively. With these assumptions, the thickness of Zn, ZnO and Ni-P layers are about 1.9, 1.7 and 3.6 μm, respectively (the reported data is an average of two measurements).

The procedure applied in this study, including the Zn electroplating, the conventional and the sonochemical hot water treatment of the zinc electroplated surface, and resulting ZnO morphologies (regardless of the true relative size) are summarized schematically in Fig. 9.

3.6. Corrosion study

The PDP measurements were carried out and the Tafel plots extracted from this electrochemical technique are shown in Fig. 10.

The electrochemical data deducted from the Tafel extrapolating including anodic and cathodic Tafel slopes (β_a, β_c), corrosion current (i_{corr}), and corrosion potential (E_{corr}) are listed in Table 4.

The positive shift in the value of the E_{OCP} (E_{OCP} is generally considered as the corrosion potential (E_{corr})) and the low current density implies that the less tendency to corrode. The results showed that the mild steel surface covered with a thin layer of zinc and the EN plated surface have lower current density (or higher polarization resistance, Rp) in comparison to the bare surface (for the Ni-P coated sample, Rp ≈ 8000 Ω cm^2). In addition, both hot water treated samples, which coated via EN plating, possess higher corrosion protection compared to other samples. The value of Rp for the samples IIA is about 25,000 Ω cm^2 and for the sample IB is about 30,000 Ω cm^2. The less tendency for the corrosion observed in these samples could be attributed to the presence of ZnO structures formed under Ni-P matrixes. The enhancement of the surface roughness created through the formation of micro- and nonosized ZnO structures results in the better adhesion of the up layer (Ni-P phase) to the base substrate. Furthermore, based on scientific reports, structures with nanometric dimensions exhibit higher electrical resistivity. This phenomenon is due to additional scattering centers, mainly from surface and grain boundaries [46]. In addition to the physical effect of the zinc oxide, its chemical effect on the improvement in corrosion resistance of samples IIA and IIB could be considered as another determining factor. This semiconductor by trapping of electron act as the barrier to ion transfer. This mechanism was proposed for the enhanced corrosion protection of organic coatings modified with ZnO pigments [39]. In our case study (metal coating), electron trapping leads to a decrease in ion transfer and consequently affect the extent of metal dissolution. Based on the open literatures, defects by improving the separation of electron-hole can enhance the adsorption and increase the visible light photo-activity [47,48]. Zheng et al. [49] indicated that different oxygen defects, including oxygen

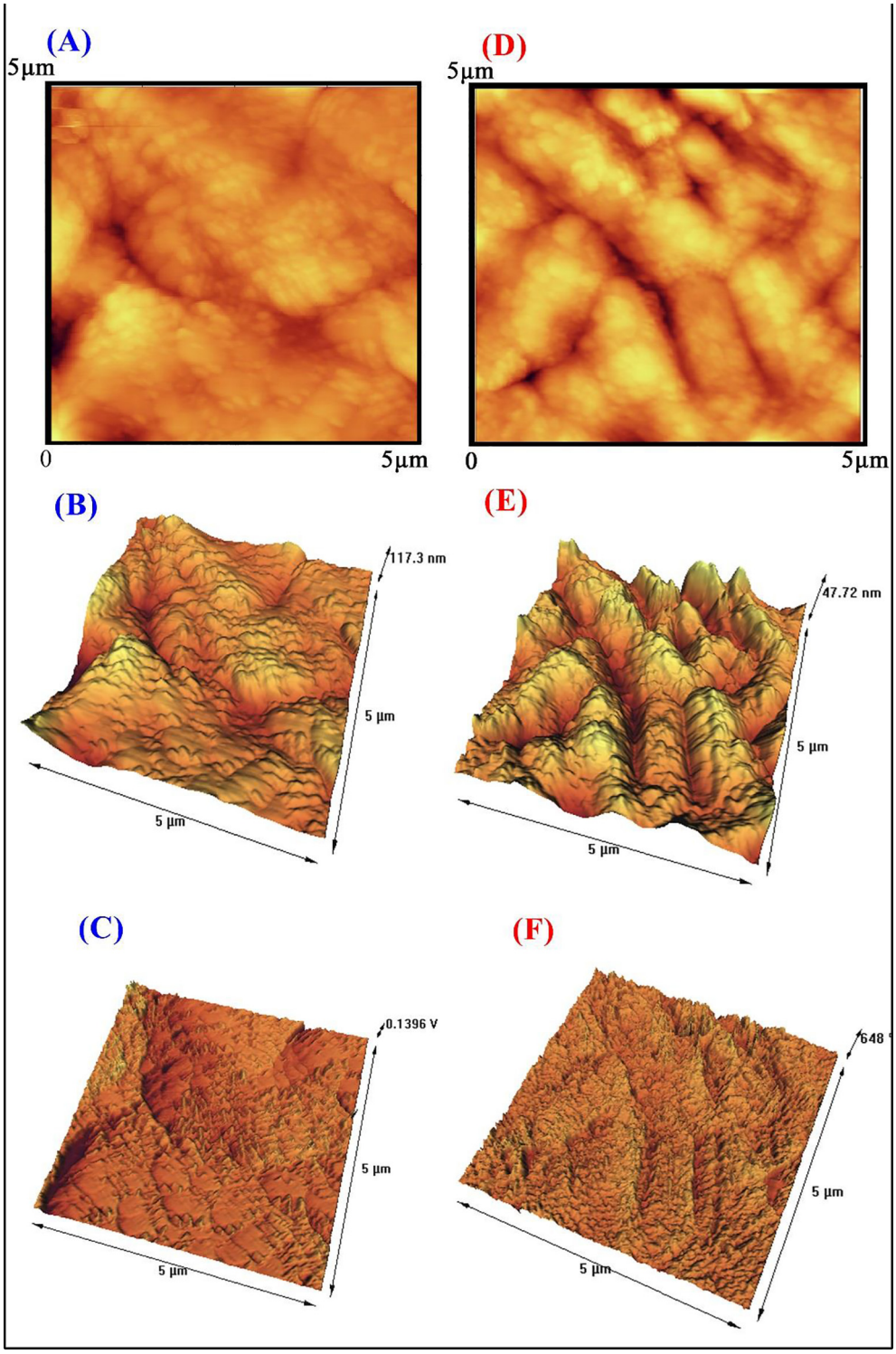

Fig. 7. AFM images including face projections ((A) and (D)), 3D topographies ((B) and (E)), and 3D phase images ((C) and (F)). Sample IA was labeled with (A), (B) and (C), and (D), (E) and (F) are attributed to the sample IB.

vacancies and interstitial oxygen had also an impact on the photo-activity of ZnO. Herein, the XPS analysis and the photoluminescence studies could be useful to identify the type of defect in the synthesized ZnO [50–52].

On the other hand, due to the presence of ZnO on the steel surface, the photo-corrosion should be considered.

ZnO as a semiconductor absorbs photons with energy greater than the band gap energy (Eg) and a large number of electrons are promoted from valence band (VB) to the conduction band (CB) of ZnO, leading to the generation of electron/hole (e^-/h^+) pairs. Most of the generated h^+ would participate in the reaction of photo-corrosion, which the overall reaction may be represented as [53–55]:

$$ZnO + 2h^+ \rightarrow Zn^{2+} + 0.5O_2 \quad (8)$$

Up to now, much works has been carried out to retard the photo-induced dissolution (photo-corrosion) of semiconductors. For instance, Su et al. showed that the polyaniline@cadmium sulfide (PANI@CdS)

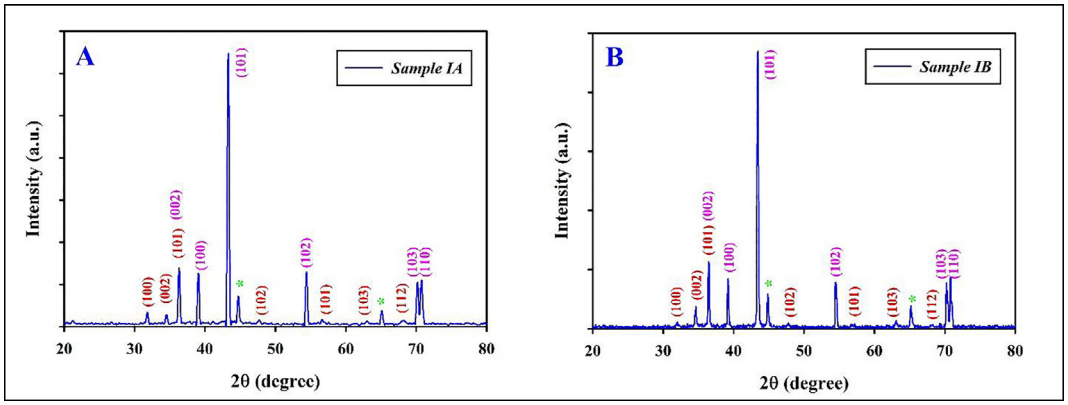

Fig. 8. The XRD patterns of: (A) sample IA, and (B) sample IB. The diffraction peaks of Zn and ZnO are marked with violet and red, respectively. The peaks marked with green stars are attributed to the Fe phase.

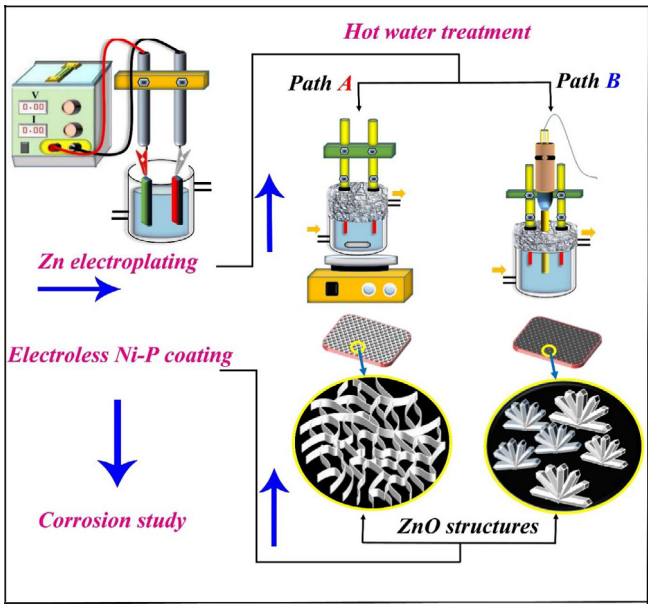

Fig. 9. The schematic representation of the Zn electrodeposition, the hot water treatment of the resulting surface via the classical and sonochemical routes, and access of the various ZnO morphologies to study the corrosion resistance of the electroless Ni-P coatings.

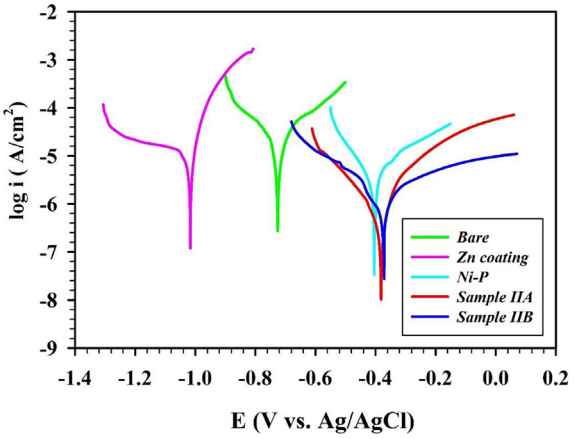

Fig. 10. Tafel plots of the samples.

core-shell nanospheres exhibited enhanced anti-photocorrosion properties [56]. In addition, photo-corrosion suppression of ZnO nanoparticles via hybridization with graphite-like carbon to enhanced photocatalytic activity was investigated by Zhang et al. [53]. The enhancement of CdS photocatalytic activity by coating Ni_2P shell was also reported in literature [57]. In the present research, coating of the ZnO film with the electroless.

Ni-P layer suppresses the photoinduced dissolution of ZnO. This film over ZnO NSs surfaces as a barrier can inhibit ZnO NSs from photocorrosion and will also remarkably increase the stability of ZnO nanoparticles. Additionally, slightly more corrosion protection of the sample IIB (compared to the sample IIA) can be assigned to the size and morphology of formed ZnO structures on this surface. The nanowall zinc oxide shapes with smaller size than flower like structures obtained in the sample IIA may lead to the improvement of mentioned physical and chemical effects of this ceramic oxide on the corrosion resistance of target coatings.

4. Conclusions

To prepare the nanostructure-supported steel surface, direct growth of ZnO structures using simple, cost effective, free seed and catalyst was aimed. Firstly, Zn electroplating technique was applied to deposit a thin layer of Zn. Appling this procedure before thermal oxidation eliminated the need of the expensive pure Zn foil (as substrate). Furthermore, as-synthesized Zn crystals, formed by this method acted as active sites on the surface, hence there was no need for the pretreatment process to convert into the ZnO phase. To oxidize the Zn layer to the ZnO phase, the electroplated samples were taken under the hot water treatment. To disclose the role of the ultrasonic irradiation on the final ZnO morphology, the hot water treatment of resulting surfaces was performed in the presence and absence of ultrasound. The results showed that the under conventional conditions flower-like structures in micro- and nano-size were formed while under sonication the ZnO nanowall network was grown. In order to evaluate the performance of resulting ZnO structures on the corrosion protection of Ni-P composite coating, as-grown ZnO structures was covered through the electroless Ni-P technique. The corrosion study of binary Ni-P coatings with and without sublayer of ZnO was evaluated by electrochemical method and the results confirmed that samples containing ZnO (samples IIA and IIB) possessed higher corrosion resistance in comparison to the sample just coated by Ni-P coating. In addition, the Ni-P surface with a sublayer of sonochemically grown ZnO structures improved the corrosion protection higher than the conventional sample. The physical and chemical effects of ZnO, including creation of the suitable roughness and better adhesion of the Ni-P film on the steel substrate and the restriction on the electron transfer in the presence of this semiconductor, were considered as the determining factors in the enhancement of the corrosion resistance. In this research, the modification of the electroplated Zn surface via the hot water treatment to produce the ZnO phase is the

Table 4
Electrochemical data obtained from the Tafel plots.

Sample	E_{corr}(V vs. Ag/AgCl)	β_a(V/dec)	β_c(V/dec)	B[a]	i_{corr}(μA/cm^2)	R_p[b] (kΩ cm^2)
Bare steel	−0.722	0.23	−0.19	0.0451	47.175	0.956
Ni-P coated steel	−0.414	0.11	−0.19	0.0302	3.415	8.855
Zn electroplated steel	−1.017	0.05	−0.63	0.0201	11.93	1.680
Sample IIA	−0.385	0.23	−0.18	0.0438	1.658	25.930
Sample IIB	−0.370	0.32	−0.17	0.0482	1.577	30.562

[a] $B = \frac{\beta_a \beta_c}{2.303(\beta_a + \beta_c)}$.

main goal (not access to the regular morphology of ZnO). However, to prevent the uncontrolled ZnO growth, changing in reaction conditions such as use of the additives (e.g. capping agents) could be examined.

Acknowledgments

The support of Ferdowsi University of Mashhad (Research and Technology) and “Iranian National Science Foundation: INSF” (no. 94026710) is appreciated. We also acknowledge the Central lab of Ferdowsi University of Mashhad.

References

[1] A. Mandal, V. Meda, W.J. Zhang, K.M. Farhan, A. Gnanamani, Synthesis, characterization and comparison of antimicrobial activity of PEG/Triton-100 capped silver nanoparticles on collagen scaffold, Colloid Surf. B 90 (2012) 191–196.
[2] M. Montazer, A. Shamei, F. Alimohammadi, Stabilized nanosilver loaded nylon knitted fabric using BTCA without yellowing, Prog. Org. Coat. 74 (2012) 270–276.
[3] G. Applerot, R. Abu-Mukh, A. Irzh, J. Charmet, H. Keppner, E. Laux, G. Guibert, A. Gedanken, Decorating parylene-coated glass with ZnO nanoparticles for antibacterial applications: a comparative study of sonochemical, microwave, and microwave-plasma coating routes, Appl. Mater. Interfaces 2 (2010) 1052–1059.
[4] R. Gottesman, S. Shukla, N. Perkas, L.A. Solovyov, Y. Nitzan, A. Gedanken, Sonochemical coating of paper by microbiocidal silver nanoparticles, Langmuir 27 (2011) 720–726.
[5] J.J. Buckley, A.F. Lee, L. Olivi, K. Wilson, Hydroxyapatite supported antibacterial Ag_3PO_4 nanoparticles, J. Mater. Chem. 20 (2010) 8056–8063.
[6] M. Moritz, M. Geszke-Moritz, The newest achievements in synthesis, immobilization and practical applications of antibacterial nanoparticles, Chem. Eng. J. 228 (2013) 596–613.
[7] Y. Liu, H.I. Kim, Characterization and antibacterial properties of genipin-cross-linked chitosan/poly(ethylene glycol)/ZnO/Ag nanocomposites, Carbohyd. Polym. 89 (2012) 111–116.
[8] L. Zhao, H. Wang, K. Huo, L. Cui, W. Zhang, H. Ni, Y. Zhang, Z. Wu, P.K. Chu, Antibacterial nano-structured titania coating incorporated with silver nanoparticles, Biomaterials 32 (2011) 5706–5716.
[9] R. Zhang, H. Olin, Carbon nanomaterials as drug carriers: real time drug release investigation, Mater. Sci. Eng., C 32 (2012) 1247–1252.
[10] S. Kokura, O. Handa, T. Takagu, T. Ishikawa, Y. Naito, T. Yoshikawa, Silver nanoparticles as a safe preservative for use in cosmetics, Nanomed. Nanotechnol. 6 (2010) 570–574.
[11] Z. Sharifalhoseini, M.H. Entezari, The new aspects of the anticorrosive ZnO@SiO_2 core–shell NPs in stabilizing of the electrolytic Ni bath and the Ni coating structure; electrochemical behavior of the resulting nano-composite coatings, J. Colloid Interface Sci. 455 (2015) 110–116.
[12] Y. Xu, H. Zhang, X. Li, W. Wang, J. Li, Ag-encapsulated single-crystalline anatase TiO_2 nanoparticle photoanodes for enhanced dye-sensitized solar cell performance, J. Alloys Compd. 695 (2017) 1104–1111.
[13] F. Zhang, J. Chen, P. Chen, Z. Sun, S. Xu, Pd nanoparticles supported on hydrotalcite-modified porous alumina spheres as selective hydrogenation catalysts, React. Kinet. Catal. 58 (2012) 1853–1861.
[14] S. Ma, R. Li, C. Lv, W. Xu, X. Gou, Facile synthesis of ZnO nanorod arrays and hierarchical nanostructures for photocatalysis and gas sensor applications, J. Hazard. Mater. 192 (2011) 730–740.
[15] H.L. Wang, L.Y. Liu, Y. Dou, W.Z. Zhang, W.F. Jiang, Preparation and corrosion resistance of electroless Ni-P/SiC functionally gradient coatings on AZ91D magnesium alloy, Appl. Surf. Sci. 286 (2013) 319–327.
[16] H. Ashassi-Sorkhabi, M. Eshaghi, Corrosion resistance enhancement of electroless Ni–P coating by incorporation of ultrasonically dispersed diamond nanoparticles, Corros. Sci. 77 (2013) 185–193.
[17] C. Buzea, I.I.P. Blandino, K. Robbie, Nanomaterials and nanoparticles: Sources and toxicity, Biointerphases 2 (2007) MR17–MR172.
[18] N. Matinise, X.G. Fuku, K. Kaviyarasu, N. Mayedwa, M. Maaza, ZnO nanoparticles via Moringa *oleifera* green synthesis: physical properties & mechanism of formation, Appl. Surf. Sci 406 (2017) 339–347.
[19] A. Diallo, B.D. Ngom, E. Park, M. Maaza, Green synthesis of ZnO nanoparticles by Aspalathus linearis: structural & optical properties, J. Alloy. Compd. 646 (2015) 425–430.
[20] X. Xu, D. Chen, Z. Yi, M. Jiang, L. Wang, Z. Zhou, X. Fan, Y. Wang, D. Hui, Antimicrobial mechanism based on H_2O_2 generation at oxygen vacancies in ZnO crystals, Langmuir 29 (2013) 5573-558.
[21] L. Zhang, Y. Jiang, Y. Ding, N. Daskalakis, L. Jeuken, M. Povey, A.J. O'Neill, D.W. York, Mechanistic investigation into antibacterial behavior of suspensions of ZnO nanoparticles against E. coli, J. Nanopart. Res. 12 (2010) 1625–1636.
[22] X. Li, Z. Wang, Y. Qiu, Q. Pan, P. Hu, 3D graphene/ZnO nanorods composite networks as supercapacitor electrodes, J. Alloy. Compd. 620 (2015) 31–37.
[23] S. Ameen, M.S. Akhtar, H.S. Shin, Growth and characterization of nanospikes decorated ZnO sheets and their solar cell application, Chem. Eng. J. 195–196 (2012) 307–313.
[24] A. Umar, M.M. Rahman, S.H. Kim, Y.-B. Hahn, Zinc oxide nanonail based chemical sensor for hydrazine detection, Chem. Commun. 2 (2008) 166–168.
[25] J.L. Zhao, X.M. Li, J.M. Bian, W.D. Yu, X.D. Gao, Structural, optical and electrical properties of ZnO films grown by pulsed laser deposition (PLD), J. Cryst. Growth 276 (2005) 507–512.
[26] M.C. Jeong, B.Y. Oh, W. Lee, J.M. Myoung, Comparative study on the growth characteristics of ZnO nanowires and thin films by metalorganic chemical vapor deposition (MOCVD), J. Cryst. Growth 268 (2004) 149–154.
[27] H.J. Ko, Y. Chen, S.K. Hong, T. Yao, MBE growth of high-quality ZnO films on epi-GaN, J. Cryst. Growth 209 (2000) 816–821.
[28] E. Ohshima, H. Ogino, I. Niikura, K. Maeda, M. Sato, M. Ito, T. Fukuda, Growth of the 2-in-size bulk ZnO single crystals by the hydrothermal method, J. Cryst. Growth 260 (2004) 166–170.
[29] Y. Natsume, H. Sakata, Zinc oxide films prepared by sol-gel spin-coating, Thin Solid Films 372 (2000) 30–36.
[30] D. Gal, G. Hodes, D. Lincot, H.W. Schock, Electrochemical deposition of zinc oxide films from non-aqueous solution: a new buffer/window process for thin film solar cells, Thin Solid Films 361–362 (2000) 79–83.
[31] D.H. Kim, J.H. Park, T.I. Lee, J.M. Myoun, Superhydrophobic Al-doped ZnO nanorods-based electrically conductive and self-cleanable antireflecting window layer for thin film solar cell, Sol. Energy Mat. Sol. 150 (2016) 65–70.
[32] R. Nandi, S.S. Major, The mechanism of growth of ZnO nanorods by reactive sputtering, Appl. Surf. Sci. 399 (2017) 305–312.
[33] J.F. Tang, Z.L. Tseng, L.C. Chen, S.Y. Chu, ZnO nanowalls grown at low-temperature for electron collection in high-efficiency perovskite solar cells, Sol. Energy Mat. Sol. 154 (2016) 18–22.
[34] C. Florica, N. Preda, A. Costas, I. Zgura, I. Enculescu, ZnO nanowires grown directly on zinc foils by thermal oxidation in air: wetting and water adhesion properties, Mater. Lett. 170 (2016) 156–159.
[35] W.K. Tan, K. Abdul Razak, K. Ibrahim, Z. Lockman, Oxidation of etched Zn foil for the formation of ZnO nanostructure, J. Alloys Compd. 509 (2011) 6806–6811.
[36] W. Tan, K.A. Razak, Z. Lockman, G. Kawamura, H. Muto, A. Matsuda, Formation of highly crystallized ZnO nanostructures by hot-water treatment of etched Zn foils, Mater. Lett. 91 (2013) 111–114.
[37] W. Tan, K. Abdul Razak, Z. Lockman, G. Kawamura, A. Matsuda, Optical properties of two-dimensional ZnO nanosheets formed by hot-water treatment of Zn foils, Solid State Commun. 162 (2013) 43–47.
[38] P. Pokorny, P. Tej, M. Kour˘il, Evaluation of the impact of corrosion of hot-dip galvanized reinforcement on bond strength with concrete – a review, Constr. Build. Mater. 132 (2017) 271–289.
[39] S. Dhoke, A. Khanna, T. Jai Mangal Sinha, Effect of nano-ZnO particles on the corrosion behavior of alkyd-based waterborne coatings, Prog. Org. Coat. 64 (2009) 371–382.
[40] J.P. Labis, M. Hezam, A. Al-Anazi, H. Al-Brithen, A.A. Ansari, A.M. El-Toni, Ronaldo Enriquez, G. Jacopin, M. Al-Hoshan, Pulsed laser deposition growth of 3D ZnO nanowall network in nest-like structures by two-step approach, Sol. Energy Mat. Sol. 143 (2015) 539–545.
[41] Z. Sharifalhoseini, M.H. Entezari, Enhancement of the corrosion protection of electroless Ni-P coating by deposition of sonosynthesized ZnO nanoparticles, Appl. Surf. Sci. 351 (2015) 1060–1068.
[42] A. Małecki, A. Micek-Ilnicka, Electroless nickel plating from acid bath, Surf. Coat. Technol. 123 (2000) 72–77.
[43] K. Hari Krishnan, S. John, K.N. Srinivasan, J. Praveen, M. Ganesan, P.M. Kavimani, An overall aspect of electroless Ni-P depositions—a review article, Metall. Mater. Trans. A 37 (2006) 1917–1926.
[44] S.H. Kim, S.W. Na, N.-E. Lee, Y.W. Nam, Y.-H. Kim, Effect of surface roughness on the adhesion properties of Cu/Cr films on polyimide substrate treated by

inductively coupled oxygen plasma, Surf. Coat. Technol. 200 (2005) 2072–2079.
[45] W. Ximei, Z. Liqun, L. Huicong, L. Weiping, Influence of surface pretreatment on the anodizing film of Mg alloy and the mechanism of the ultrasound during the pretreatment, Surf. Coat. Technol. 202 (2008) 4210–4217.
[46] H. Marom, M. Eizenberg, The effect of surface roughness on the resistivity increase in nanometric dimensions, J. Appl. Phys. 99 (2006) 123705.
[47] A. Mclaren, T.V. Solis, G. Li, S.C. Tsang, Shape and size effects of ZnO nanocrystals on photocatalytic activity, J. Am. Chem. Soc. 131 (2009) 12540–12541.
[48] M.Y. Guo, A.M.C. Ng, F. Liu, A.B. Djurišić, W. Kin Chan, H. Su, K.S. Wong, Effect of native defects on photocatalytic properties of ZnO, J. Phys. Chem. C 115 (2011) 11095–11101.
[49] Y. Zheng, C. Chen, Y. Zhan, X. Lin, Q. Zheng, K. Wei, J. Zhu, Y. Zhu, Luminesce and photocatalytic activity of ZnO nanocrystals: correlation between structure and property, Inorg. Chem. 46 (2007) 6675–6682.
[50] X. Zhang, J. Qin, Y. Xue, P. Yu, B. Zhang, L. Wang, R. Li, Effect of aspect ratio and surface defects on the photocatalytic activity of ZnO nanorods, doi:10.1038/srep04596.
[51] M. Khenfouch, M. Baïtoul, M. Maaza, White photoluminescence from a grown ZnO nanorods/graphene hybrid nanostructure, Opt. Mater. 34 (2012) 1320–1326.
[52] B.D. Ngom, T. Mpahane, N. Manyala, O. Nemraoui, U. Buttner, J.B. Kana, A.Y. Fasasi, M. Maaza, A.C. Beye, Structural and optical properties of nano-structured tungsten-doped, ZnO thin films grown by pulsed laser deposition, Appl. Surf. Sci. 255 (2009) 4153–4158.
[53] L. Zhang, H. Cheng, R. Zong, Y. Zhu, Photocorrosion suppression of ZnO nanoparticles via hybridization with graphite-like carbon and enhanced photocatalytic activity, J. Phys. Chem. C 113 (2009) 2368–2374.
[54] R.T. Sapkal, S.S. Shinde, T.R. Waghmode, S.P. Govindwar, K.Y. Rajpure, C.H. Bhosale, Photo-corrosion inhibition and photoactivity enhancement with tailored zinc oxide thin films, J. Photochem. Photobiol., B 110 (2012) 15–21.
[55] L. Yu, W. Chen, D. Li, J. Wang, Y. Shao, M. He, P. Wang, X. Zheng, Inhibition of photocorrosion and photoactivity enhancement for ZnO via specific hollow ZnO core/ZnS shell structure, Appl. Catal., B 164 (2015) 453–461.
[56] C. Wang, L. Wang, J. Jin, J. Liu, Y. Li, M. Wu, L. Chen, B. Wang, X. Yang, B.-L. Su, Probing effective photocorrosion inhibition and highly improved photocatalytic hydrogen production on monodisperse PANI@CdS core-shell nanospheres, Appl. Catal. B 188 (2016) 351–359.
[57] W. Zhen, X. Ning, B. Yang, Y. Wu, Z. Li, G. Lu, The enhancement of CdS photocatalytic activity for water splitting via anti-photocorrosion by coating Ni_2P shell and removing nascent formed oxygen with artificial gill, Appl. Catal., B 221 (2018) 243–257.